Morphological Features of Blown High-Density Polyethylene Films

YONG-MAN KIM,[1] CHUL-HWAN KIM,[1] JUNG-KI PARK,[1,*] JUNG-WHAN KIM,[2] and TAE-IK MIN[2]

[1]Department of Chemical Engineering, Korea Advanced Institute of Science and Technology, 373-1, Kusung-dong, Yusung-gu, Daejon, 305-701, South Korea; [2]Central Research Center, Hanwha Chemical Corporation, 6, Shinsung-dong, Yusung-gu, Daejon, 305-345, South Korea

SYNOPSIS

The blown films of high-density polyethylenes with unimodal and bimodal molecular weight distribution were prepared under several processing conditions, and their morphologies were extensively characterized. The high molecular weight tail (MW > ~ 10^6) of the molecular weight distribution seems to play a critical role on the morphology of blown high-density polyethylene films irrespective of the molecular weight distribution mode of the resins. As the content of high molecular weight species increased, the tendency for high stress-crystallization increased and the network structure of lamellar stacks was better developed. The intercrystalline connectivity along the normal direction of lamellar stacks was higher than that along the transverse direction of lamellar stacks. © 1996 John Wiley & Sons, Inc.

INTRODUCTION

Blown high-density polyethylene (HDPE) film is one of the most widely used polymeric materials. The bulk property of blown HDPE film is usually determined by the morphology such as crystallinity, stacked lamellar crystalline morphology, intercrystalline connectivity, and preferred orientation. For these reasons, the morphological characterization of blown HDPE films is of considerable interest both from the standpoint of scientific curiosity and commercial significance. Many efforts have been performed to understand the morphology of blown HDPE films and to interrelate the morphology with the bulk properties of the blown films.[1-26]

The morphology of blown HDPE films generally depends on the overall processing parameters such as extrusion temperature, draw ratio (DR), blow-up ratio (BUR), and frost-line height (FLH) as well as on the molecular structural parameters such as molecular weight and branching. Pearson[1] and Pearson and Petrie[2,3] attempted at first to determine the factors relevant to the blowing process from a theoretical viewpoint. Later, several authors reported theoretical and experimental investigations considering the kinematics, dynamics, heat transfer, and bubble stability in the tubular blown-film process.[4-9] However, in spite of the importance, only few studies concerning the influence of molecular structure on the morphology of blown HDPE films have been made.

In the 1980s, new HDPE film resins with a bimodal molecular weight distribution (bimodal HDPE) were developed and have gained an increasing share of the marketplace.[27-30] Bimodal HDPE resin has greatly improved properties, especially the film dart drop impact strength compared to conventional unimodal molecular weight distribution HDPE (unimodal HDPE) resin of similar melt index and density. This implies that the morphology of the blown bimodal HDPE film is different from that of the blown unimodal HDPE film. Therefore, thorough morphological investigation of these two types of HDPE films prepared under the same processing conditions can help in understanding the effect of molecular structure on the morphology of blown HDPE films. In this article, the blown films of the

* To whom correspondence should be addressed.

Journal of Applied Polymer Science, Vol. 61, 1717-1729 (1996)
 CCC 0021-8995/96/101717-13

HDPE resins with unimodal and bimodal molecular weight distribution were prepared using a commercial tubular blown film extruder, and the morphological features of these films were extensively investigated.

EXPERIMENTAL

Materials

Four commercial HDPEs, labeled BH, UH, BM, and UM, were used in this study. The melt index, density, average molecular weight, polydispersity, average short-chain branching content, and branch type of the resins are summarized in Table I. The molecular weight distributions of the polymers are shown in Figure 1. The BH and BM resins have a bimodal molecular weight distribution (MWD), while the UH and UM resins have a unimodal MWD.

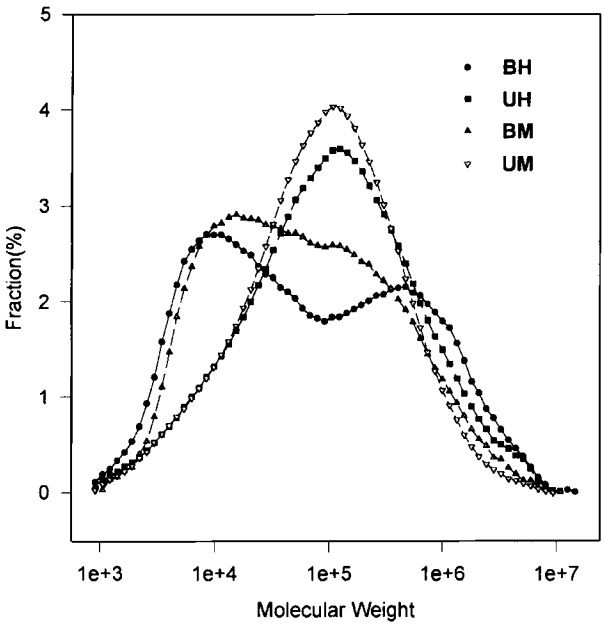

Figure 1 Gel permeation chromatograms of the HDPE resins.

Blown Film Preparation

Films were prepared using a 40 mm Yoo Jin Engineering tubular blown HDPE film equipment. It consists of a full flight screw with an L/D of 25 to 1, a 50 mm spiral die with a die gap of 1 mm, an internal bubble stabilizer, an air ring, nip rolls, and a take-up device. In this study, the extrusion motor speed was fixed at 1050 rpm, and the extrusion temperature was fixed at 165, 180, 190, 200, and 200°C for cylinder zones 1, 2, and 3, head, and die, respectively. Processing conditions were chosen to obtain films that were approximately 20 μm in thickness for measurements of the mechanical properties of the films. For the BH and UH resins, three films were blown from each resin under the three sets of processing parameters: DR, BUR, and FLH. Blowing condition 1 is a commercially typical one. For

Table I Characteristics of the HDPE Resins

	Resin			
Characteristics	BH	UH	BM	UM
Melt Index (g/10 min)				
$I_{2.16}$[a]	0.05	0.07	0.32	0.42
$I_{21.6}$[b]	8.5	10.5	27.7	32.6
Density[c] (g/cm^3)	0.9535	0.9532	0.9551	0.9535
M_n	12,149	21,468	15,220	22,535
M_w	363,889	331,655	235,422	219,449
M_w/M_n	30.0	15.5	15.5	9.7
Fraction (%)				
MW > 6×10^5	18.9	13.6	10.1	8.20
MW > 10^6	11.2	8.67	6.07	4.37
Comonomer type	1-Butene	1-Butene	1-Butene	1-Hexene
SCB[d] content, CH_3/1000 C	2.0	1.9	2.1	1.8

[a] ASTM D 1238 (condition E).
[b] ASTM D 1238 (condition F).
[c] ASTM D 1505.
[d] Short-chain branching.

Table II Blowing Conditions of the Films

		Frost-line		
UH-1	5.0	7.5	53	20
UH-2	2.5	13.8	54	22
UH-3	2.5	14.8	25	23
BM-3	2.5	13.7	25	24
UM-3	2.5	14.4	25	23

blowing condition 2, the stretching along the machine direction (MD) was increased while the stretching along the transverse direction (TD) was decreased compared to those of blowing condition 1. Blowing condition 3 is very similar to blowing condition 2 except for the lower FLH. In the case of the BM and UM resins, it was impossible to produce proper films due to the lack of bubble stability at blowing conditions 1 and 2, since the melt stability under these processing conditions was poor. A detailed summary of the films prepared is presented in Table II.

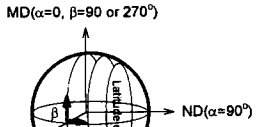

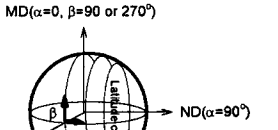

Characterization of the Morphology of Films

The melting behavior of the films was analyzed by differential scanning calorimetry (DSC) using a DuPont Thermal Analyst 2100 Model at a heating rate of 10°C/min in a nitrogen atmosphere. The melting endotherms were recorded by heating the samples from 30 to 160°C. The degree of crystallinity from the calorimetric data was calculated using 69 cal/g for the completely crystalline polyethylene.[31]

The preferred orientation of the films was determined using polarized infrared absorption and wide-angle X-ray diffraction. The infrared dichroic measurements were made on Bomem-MB-100 FTIR spectrometer equipped with a Bio-Rad PT polarizer. Pole figures of the diffraction planes for the films were obtained using Rigaku D/MAX-III C(3 kW). Detailed information on the pole figure measurement procedure was presented elsewhere.[32,33] Twenty-five sheets of films were carefully stacked to give a 500 μm in total thickness approximately and clamped so as to maintain their sample directions parallel. A specimen was cut from the original stacks using a disk cutter with a diameter of 32 mm and the edge of the disk specimen was glued with a water-based glue. All the X-ray measurements were performed using nickel-filtered CuKα radiation produced at 40 kV and 45 mA. The Decker transmission and Schulz reflection method were used for low and high α angles, respectively. The connection angle was 30°. Measurement conditions were as follows: α angle variation, 0–90°; β angle variation, 0–360°; α and β angle step, 10°; β angle speed, 190°/min; and γ oscillation, 10 mm. The mean-square cosines of the angle between the crystallographic axes and the sample reference directions, MD, TD, and normal direction (ND), were calculated with internal software of the diffractometer. The intensity data were corrected for background scattering and absorption.

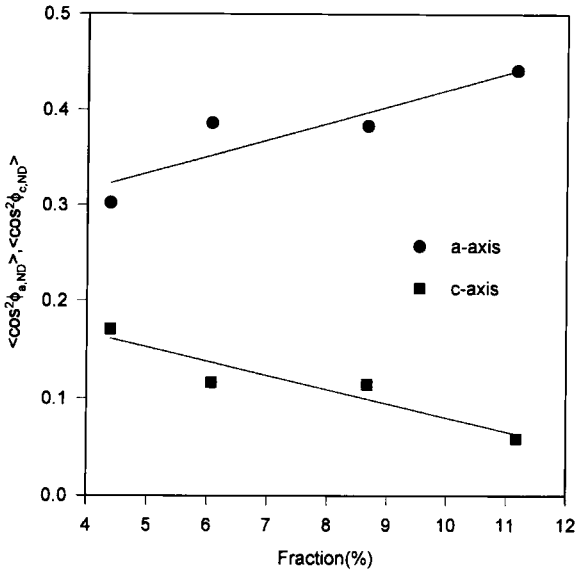

Figure 4 The mean-square cosines of the angle between the a-axis and the c-axis and the normal direction, $\langle\cos^2\phi_{a,ND}\rangle$ and $\langle\cos^2\phi_{c,ND}\rangle$, of the films against the content of high molecular weight species > (MW > 10^6) of the resins.

The crystalline morphology of the three reference planes, the MD–TD, MD–ND, and TD–ND planes, and the brittle fracture specimen of the films was observed by a scanning electron microscope (SEM). A Phillips SEM 535M was used. A cross section of

Table III Dichroic Ratios (MD/TD) of Crystallographic Axes

	Dichroic Ratio (MD/TD)					
	a-Axis		b-Axis		c-Axis	
Film	Pole Figure[a]	IR[b]	Pole Figure	IR	Pole Figure	IR
BH-1	1.125	1.105	0.380	0.463	1.305	1.318
BH-2	0.559	0.621	0.254	0.421	1.646	1.617
BH-3	1.035	0.978	0.234	0.454	1.456	1.444
UH-1	1.338	1.159	0.352	0.454	1.194	1.402
UH-2	0.544	0.667	0.332	0.478	1.597	1.707
UH-3	1.123	1.059	0.242	0.547	1.401	1.412
BM-3	1.436	1.369	0.216	0.479	1.290	1.422
BM-3	1.800	1.819	0.245	0.480	1.058	1.199

[a] $\langle\cos^2\phi_{i,MD}\rangle/\langle\cos^2\phi_{i,TD}\rangle$.
[b] A_{MD}/A_{TD}.

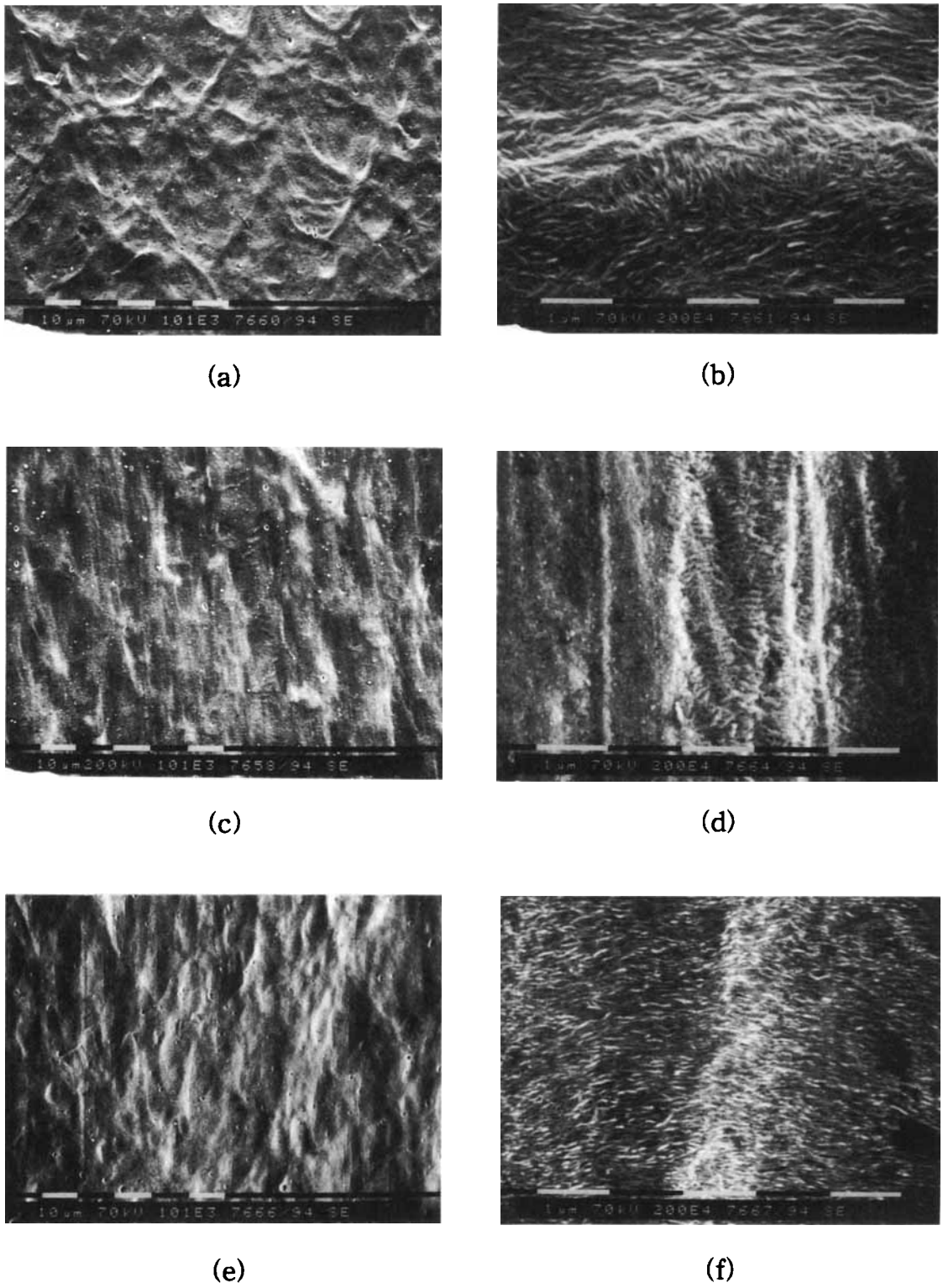

Figure 5 Scanning electron micrographs of the normal plane of the resin BH films (MD ↑, TD →): (a) BH-1, 1000×; (b) BH-1, 20,000×; (c) BH-2, 1000×; (d) BH-2, 20,000×; (e) BH-3, 1000×; (f) BH-3, 20,000×.

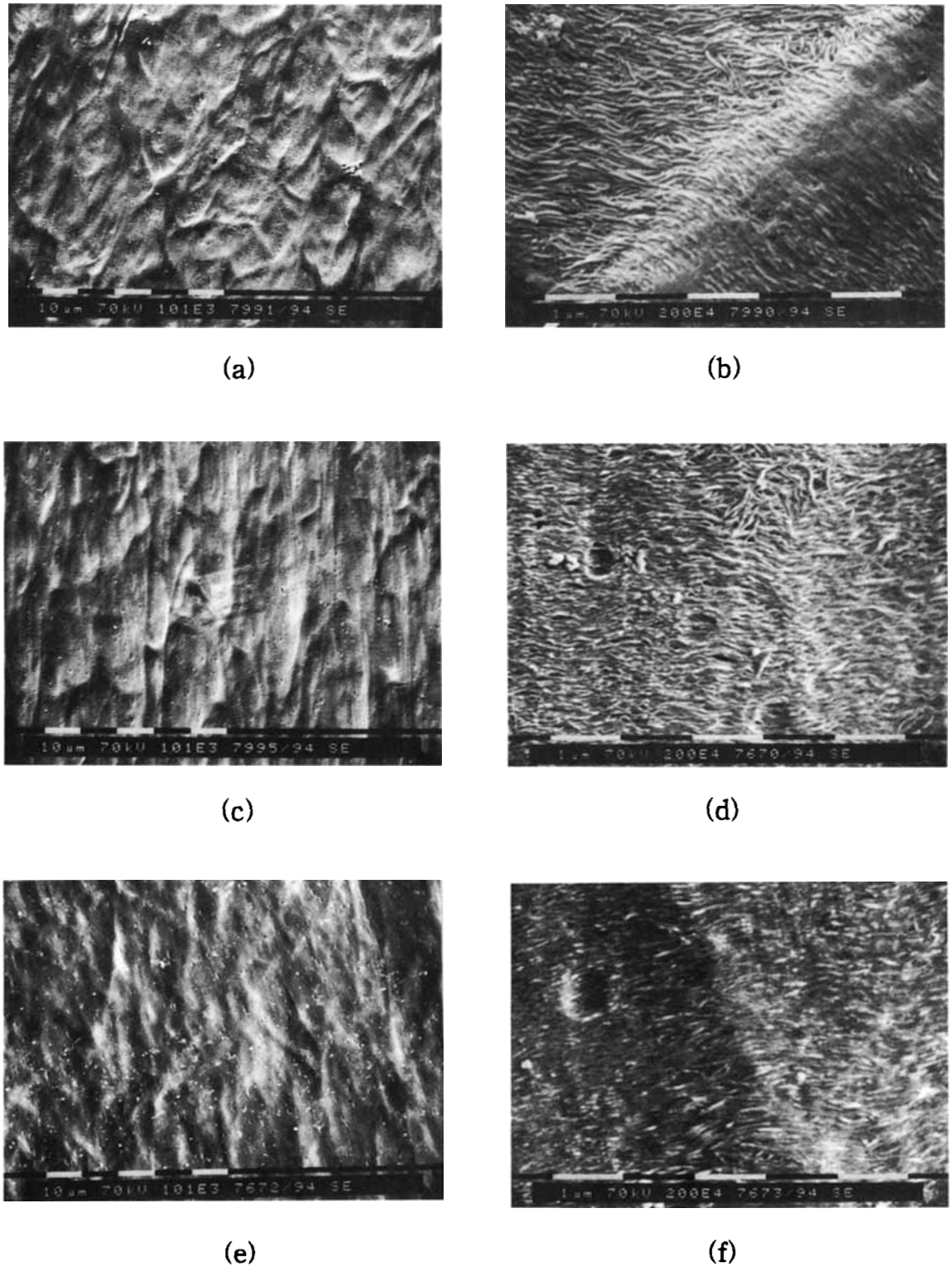

Figure 6 Scanning electron micrographs of the normal plane of the resin UH films (MD ↑, TD →): (a) UH-1, 1000×; (b) UH-1, 20,000×; (c) UH-2, 1000×; (d) UH-2, 20,000×; (e) UH-3, 1000×; (f) UH-3, 20,000×.

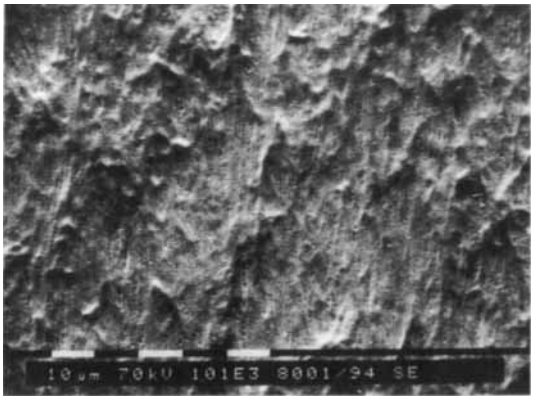

(a)

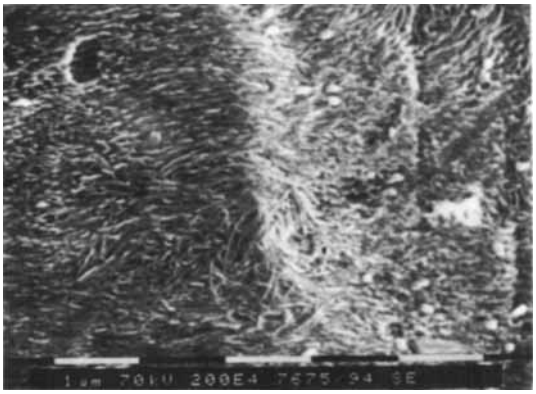

(b)

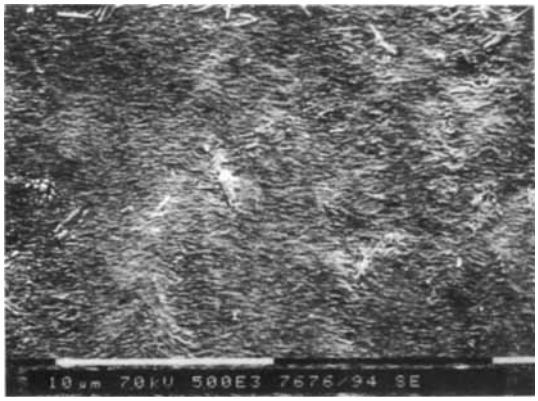

(c)

Figure 7 Scanning electron micrographs of the normal plane of the resin BM and UM films (MD ↑, TD →): (a) BM-3, 1000×; (b) BM-3, 20,000×; (c) UM-3, 5000×.

the films was prepared by cryo-ultramicrotoming with a diamond knife at −130°C. The specimens were etched with a 0.7 wt % solution of $KMnO_4$ in a 2 : 1 (v/v) mixture of concentrated sulfuric acid and 98% phosphoric acid for 1 h at room temperature. The etched specimens were washed with a 2 : 7 mixture of concentrated sulfuric acid and water, washed with water again, and freeze-dried. They were mounted on SEM stubs with double-stick tape and sputter-coated with gold. Accelerating voltage, probe current, and tilt angle were 7 kV, 3×10^{-11} mA, and 30°, respectively.

The tie molecule density of the films along the MD and TD was evaluated from brittle fracture stress measurements proposed by Brown and Ward.[34] The brittle fracture stress of the films was measured using an Instron testing machine equipped

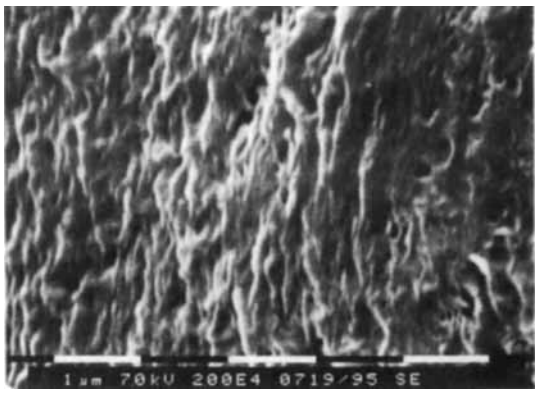

(a)

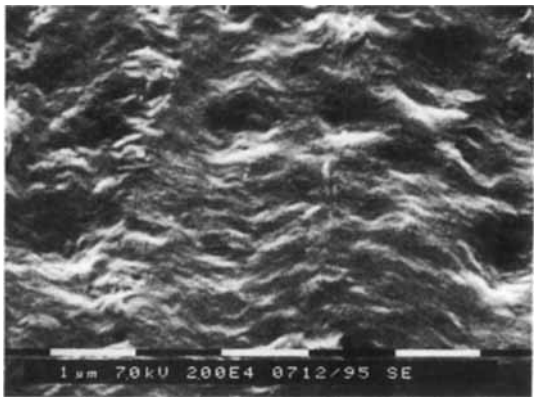

(b)

Figure 8 Scanning electron micrographs of cross sections of the UH-1 film: (a) TD(↑)–ND(→) plane; (b) MD(↑)–ND(→) plane.

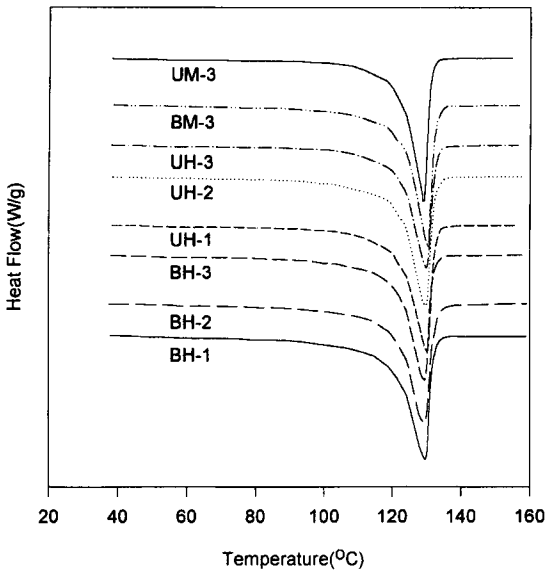

Figure 9 DSC melting endotherms of the films.

with modified grips. The ASTM D 1708 dog-bone-type tensile specimens were cut out of the films and gripped firmly by the jaws which were mounted inside the reservoir of liquid nitrogen. The specimens were conditioned for 10 min and deformed at a crosshead speed of 500 mm per min.

RESULTS AND DISCUSSION

Preferred Orientation

The development of molecular orientation in the crystalline phase of blown HDPE film can be conveniently determined by investigating the alignment of its unit cell. Figures 2 and 3 show the normalized intensity profiles of the (200) and (020) poles, i.e., *a*- and *b*-axis distribution, as a function of the α and β angles. In these figures, the relationship between the α and β angles and the sample reference directions (MD, TD, and ND) is also illustrated. The major tick mark of the abscissa indicates the α angle variations with a stepwise increment of 10°, and the minor tick mark indicates the β angle variations from 0 to 350° at a given α angle.

For the BH-1 film prepared from the high molecular weight (HMW) bimodal BH resin at blowing condition 1, as the α angle increases at β = 90 or 270°, the intensity of the (200) pole increases very slowly up to α = 40° and then steeply increases and shows a maximum at α = 70°. With a further increase in α angle, there is a slight decrease in intensity. The intensity variation of the (200) pole with the β angle is very small in the range of α = 0–40°. However, at a higher α angle, the intensity of the

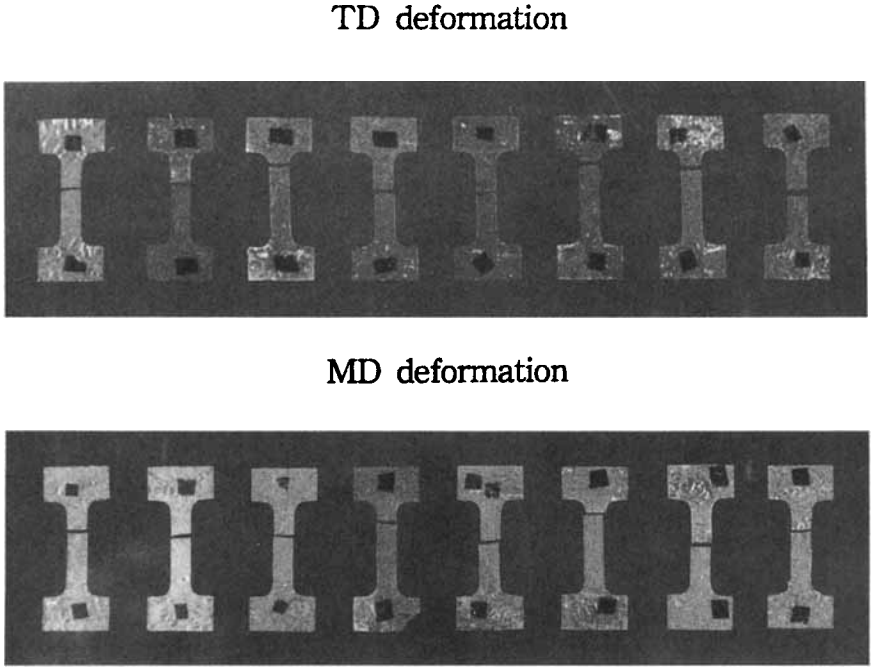

Figure 10 Photograph of the brittle fracture specimens of the films.

Table IV Brittle Fracture Stress and Calculated Tie Molecule Density of the Films

	Brittle Fracture Stress (Gpa)		Tie Molecule Density[a] (Fraction)							
			$\beta = 0.1, c = 20$		$\beta = 0.1, c = 50$		$\beta = 0.2, c = 20$		$\beta = 0.2, c = 50$	
Film	MD	TD	MD	TD	MD	TD	MD	TD	MD	TD
BH-1	0.1365	0.1185	0.066	0.054	0.206	0.176	0.019	0.013	0.090	0.074
BH-2	0.1685	0.1045	0.088	0.044	0.261	0.152	0.030	0.008	0.117	0.062
BH-3	0.1375	0.1115	0.067	0.049	0.208	0.164	0.020	0.011	0.090	0.068
UH-1	0.1265	0.1160	0.059	0.052	0.189	0.171	0.016	0.012	0.081	0.072
UH-2	0.1590	0.0970	0.082	0.039	0.245	0.139	0.027	0.006	0.109	0.056
UH-3	0.1305	0.1100	0.062	0.048	0.196	0.161	0.017	0.010	0.084	0.067
BM-3	0.1285	0.1155	0.061	0.052	0.193	0.170	0.017	0.012	0.083	0.072
UM-3	0.1215	0.1110	0.056	0.049	0.181	0.163	0.014	0.011	0.077	0.068

[a] Tie molecule density (Ref. 34), $f_T = (C\sigma_F - \beta E_{iso})/\beta(E_T - E_{iso})$, where C is the stress concentration; σ_F, the brittle fracture stress; β, the constant of proportionality, E_{iso} and E_T, the Young's modulus for van der Waals' bonds (8 Gpa) and tie molecule (300 Gpa), respectively.

(200) pole follows a periodic function with the maxima at $\beta = 90$ and 270° and the minima at $\beta = 0$ and 180°. These results represent that the a-axes are preferentially oriented along the ND and that the a-axes have a preferential orientation to the MD than to the TD at a given tilt angle ($90° - \alpha$) to the ND. This indicates that the orientation occurred under the high-stress crystallization proposed by Maddams and Preedy.[16] It is also found that the b-axes of the BH-1 film are mostly perpendicular to the MD and have a preferential orientation to the ND in the ND–TD plane. From the preferred orientation of the a-axes and b-axes of the BH-1 film and the orthorhombic structure of polyethylene, it seems that the c-axes of the film BH-1 are mostly perpendicular to the ND and, thus, to the MD–TD plane.

In the case of the BH-2 film, the a-axes and b-axes are mostly perpendicular to the MD. It is certain that the orientation occurred under the very high stress crystallization. This implies that the c-axis of the BH-2 film seems to show a higher preferential orientation along the MD compared to that of the BH-1 film, i.e., the MD oriented lamellar stack is dominant. The difference in the preferred orientation between the BH-1 and BH-2 films is caused by the differences in DR and BUR. For the BH-2 film, the stretching in the MD is increased and the stretching in the TD is decreased compared to those of the BH-1 film. Compared to the BH-2 film, the BH-3 film has a weak tendency for high-stress crystallization orientation. This is attributed to the lower FLH of the BH-3 film, which was already explained by Maddams and Preedy.[15,16]

For the films prepared from the HMW unimodal UH resin, it is apparent that the dependency of the preferred orientation on blowing conditions is similar to that of the HMW bimodal BH resin. However, the maximum of the intensity of the a-axes for the HMW unimodal UH resin films is positioned at a lower α angle than that of the corresponding HMW bimodal BH resin films. This indicates that the preferred orientation of the bimodal BH resin films is more dependent on the high-stress crystallization than on that of the unimodal resin UH films.

In the case of the medium molecular weight (MMW) bimodal resin BM-3 film and the unimodal resin UM-3 film, the high-stress crystallization orientation was considerably diminished compared to the corresponding HMW resin BH-3 and UH-3 films. Especially, the UM-3 film has a great tendency for low-stress crystallization orientation.

The mean-square cosines of the angle, $\langle \cos^2\phi_{ij} \rangle$, between a crystallographic axis (i = a- and b-axes) of the orthorhombic crystallites of polyethylene and the sample reference directions (j = ND, MD, TD) were calculated by the well-known method.[32,33,35] The mean-square cosines of the angle between the c-axis and the sample reference directions, $\langle \cos^2\phi_{cj} \rangle$, were calculated from $\langle \cos^2\phi_{aj} \rangle + \langle \cos^2\phi_{bj} \rangle + \langle \cos^2\phi_{cj} \rangle = 1$. IR dichroic ratios were also measured to obtain the preferred orientation of each crystallographic axis. The observed absorption bands are as follows: CH_2 rocking mode doublet at 719/730 cm^{-1}; CH_2 bending mode doublet at 1462/1473 cm^{-1}; CH_2 wagging mode at 1175 cm^{-1}; and CH_2 twisting mode at 1050 cm^{-1}. The transition moment direction is parallel to the a-axis for the peaks at 730 and 1473

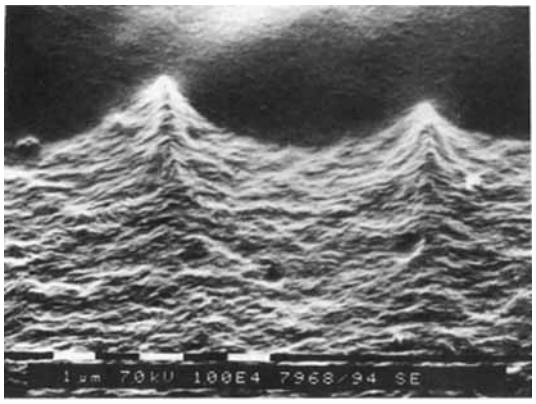

(a)

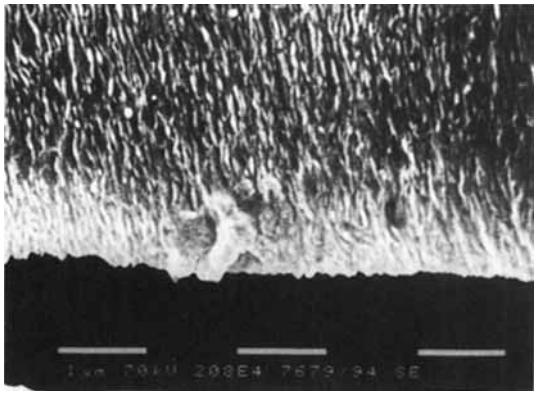

(b)

Figure 11 Scanning electron micrographs of the brittle fracture specimens of the BH-2 film: (a) MD tensile deformation (MD ↑, TD →); (b) TD tensile deformation (TD ↑, MD →).

cm^{-1}, to the *b*-axis for the peaks at 719 and 1462 cm^{-1}, and to the *c*-axis for the peaks at 1050 and 1175 cm^{-1}.[36] Data processing for the resolution of the doublet peaks was carried out by the previous method reported by Zerbi et al.[37] and Kissin.[38]

Dichroic ratios obtained by the pole figure measurements are in good agreement with those of the polarized IR spectroscopy measurements, as shown in Table III. The effects of processing conditions and resin types on the average orientation of crystallographic axes for all the films are clearly shown in Table III. From the level of molecular structure, it is very important to examine the effect of resin types on the preferred orientation of the crystallographic axes for the films. It is reasonable to expect that the high molecular weight tail of the molecular weight distribution is important, since it is responsible for the formation of the small number of the extended-chain core fibrils which subsequently act as nuclei for the lamellar crystallization of the remainder of the material. For the four films, BH-3, UH-3, BM-3, and UM-3, the mean-square cosines of the angle between the *a*- and *c*-axes and the ND are plotted against the content of high molecular weight components of which the molecular weights are greater than 10^6 in Figure 4. This suggests that the degree of stress may be determined mainly by the high molecular weight content of the resins irrespective of the resin types.

Lamellae and Lamellar Stacks

The typical scanning electron micrographs of the normal plane for the films are presented in Figures 5–7. The MD and TD are vertical and horizontal directions of the micrographs, respectively. These micrographs show morphological features that are responsible for the observed differences in the previous pole figure patterns. The low magnification (1000×) micrographs clearly reveal the superstructure, i.e., the organization of lamellar stacks, of the films. The lamellar structure of the films is well shown in the higher magnification (20,000×) micrographs taken by zooming up around the well-developed lamellar stacks in the micrographs of 1000× magnification.

The scanning electron micrographs for the three films prepared from the HMW bimodal BH resin are given in Figure 5. The BH-1 film has an obvious stacked lamellar morphology, as shown in Figure 5(b). The lamellae are curved, well-defined, and or-

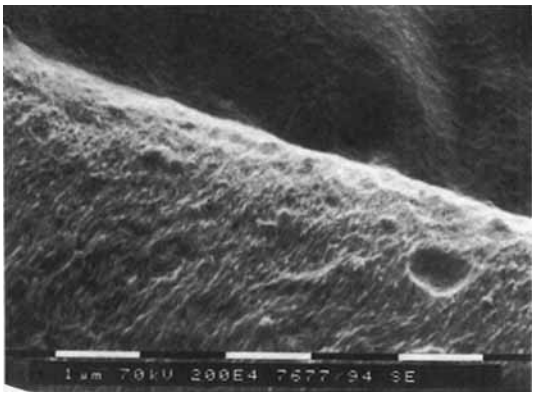

Figure 12 Scanning electron micrograph of the brittle fracture specimen of the BH-2 film [tensile deformation along 45° to the MD(↘)].

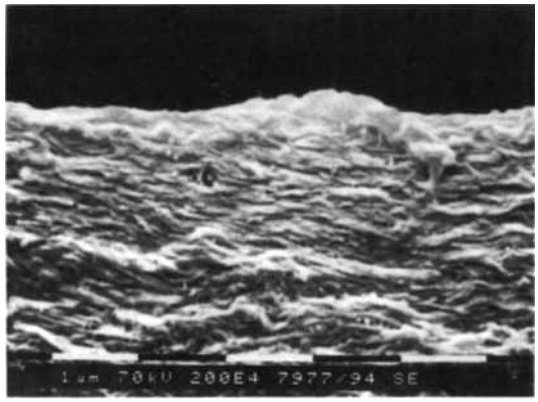

(a)

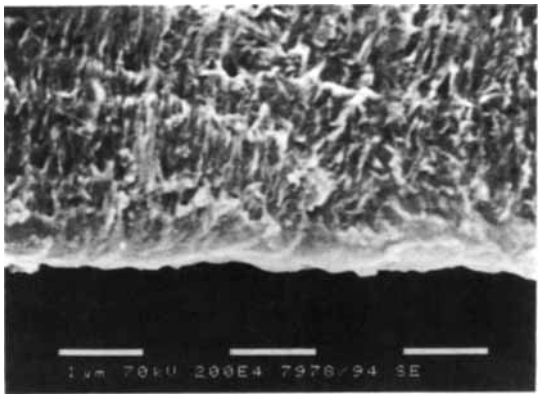

(b)

Figure 13 Scanning electron micrographs of the brittle fracture specimens of the UM-3 film: (a) MD tensile deformation (MD ↑, TD →); (b) TD tensile deformation (TD ↑, MD →).

ganized to form lamellar stacks. The organization of lamellar stacks is clearly shown in Figure 5(a). The well-developed long lamellar stacks (network lamellar stack) are curled and interconnected, forming a network just like a fish net in the film. These lamellar stacks are about 2 μm wide and 5–20 μm long between intersections or junctions with other stacks in the network. The normals of these lamellar stacks are rather randomly distributed along the film plane (the MD–TD plane). In the interstices of the network, the lamellar stacks (interstitial lamellar stack) with a narrower width are developed, and their normals seem to be preferentially oriented to the MD.

Compared to the BH-1 film, the BH-2 film shows the lamellar stacks to be highly ordered with their normals along the MD and the overall lamellar organization to be more coherent, as shown in Figure 5(c) and (d). The structure of the BH-2 film seems to be very similar to the shish-kebab morphology reported by Keller et al.[39,40] They demonstrated that high molecular weight components contribute to the formation of extended chain fibrils which constitute the backbone of the shish kebabs in the melt spinning of HDPE and pointed out that this feature is general to the melt extrusion process. Figure 5(e) and (f) shows that the normals of lamellar stacks of the BH-3 film have a preferential orientation to the MD, although the degree of the MD orientation is lower than that of the BH-2 film. On the whole, the above variations of the orientation of lamellar stacks prepared from the BH resin with processing conditions are in good agreement with the results reported previously.[20,24,26]

In Figure 6, the scanning electron micrographs for the three films prepared from the HMW unimodal UH resin are given. The UH-1 film also shows the network structure which consists of the network lamellar stacks and interstitial lamellar stacks [Fig. 6(a) and (b)]. However, compared to the BH-1 film, the UH-1 film has a higher preferential orientation of the network lamellar stacks along the MD. It is apparent from Figure 6 that the dependency of the structure of the films prepared from the HMW unimodal UH resin on blowing conditions is quite similar to that of the HMW bimodal BH resin.

The scanning electron micrographs obtained for the MMW resin films are given in Figure 7. For the MMW bimodal resin BM-3 film, it is found that the well-developed lamellar stacks are rather randomly oriented compared to the HMW bimodal resin BH-3 film. However, these are relatively short, curved, and highly segmented. In addition, interconnections between them are rare. The development of the network structure is not clearly found for the MMW unimodal resin UM-3 film. The UM-3 film has primarily lamellar stacks oriented with their normals parallel to the MD. It becomes thus quite evident that the one-sided consideration either on the orientation of crystallographic axis or lamellar stacks is inadequate to characterize the morphology of the blown HDPE films and to correlate the morphology with mechanical properties.

Films were sectioned perpendicular to the MD and TD and etched to examine the lamellar morphology through the film thickness, i.e., the morphology of the MD–ND and TD–ND planes. For all the films, the morphology was very similar. The typical scanning electron micrographs of the MD–

ND and TD–ND planes for the UH-1 film are presented in Figure 8. The sample directions are noted in the figure caption. It is clear that lamellae did preferentially grow along the TD and ND. This is in agreement with the results of the pole figure analysis.

Crystallinity

The melting behavior of the films was studied with a differential scanning calorimeter. There is no significant differences in the degree of crystallinity (68 $\pm$ 3%) and peak melting temperature (129.8 $\pm$ 0.7°C) between all the films, as shown in Figure 9. This feature is in good agreement with the results reported previously.[26]

Tie Molecules (Intercrystalline Connectivity)

The brittle fracture tensile stress of the films was measured for the calculation of the tie molecule density of the films according to the method proposed by Brown and Ward.[34] As shown in Figure 10, the failure mode was found to be an instantaneous brittle fracture. The brittle fracture stress and calculated tie molecule density of the films are listed in Table IV. The orientation of lamellar stacks is well revealed in the scanning electron micrographs, as shown in Figure 11. For the MD tensile deformation, it is clear that fracture occurred along the basal plane of lamellae, i.e., perpendicular to the lamellar stack axis, and it seems to include core fibrils, as shown in Figure 11(a). However, for the TD tensile deformation, fracture occurred along the lamellar stack axis, i.e., between lamellar stacks. The fracture stress of the TD tensile deformation is significantly lower than that of the MD tensile deformation, as shown in Table IV. When the tensile stress is applied along 45° to the MD, the fracture occurred along the MD, i.e., between lamellar stacks, as shown in Figure 12. These fracture results clearly indicate that the boundary between lamellar stacks is weak. Another interesting feature is found from the scanning electron micrographs shown in Figure 13: that the lamellae of the film UM-3 are more separated than are those of the other films and thin tie fibrils are formed between lamellae [Fig. 13(a)]. This implies that the lamellae of the UM-3 film are less stable. It seems therefore that the most pertinent feature of the crystalline microstructure of the blown HDPE films is the organization of lamellae into stacks, the orientation distribution of these lamellar stacks, and the presence of the network structure.

Support of this work by Hanwha Chemical Corp. is gratefully acknowledged.

REFERENCES

1. J. R. A. Pearson, *Mechanical Principles of Polymer Melt Processing,* Pergamon, Oxford, 1966.
2. J. R. A. Pearson and C. J. S. Petrie, *J. Fluid Mech.,* **40,** 1 (1970).
3. J. R. A. Pearson and C. J. S. Petrie, *J. Fluid Mech.,* **42,** 609 (1970).
4. R. Farber and J. Dealy, *Polym. Eng. Sci.,* **14,** 435 (1974).
5. C. D. Han and J. Y. Park, *J. Appl. Polym. Sci.,* **19,** 3257 (1975).
6. C. D. Han and J. Y. Park, *J. Appl. Polym. Sci.,* **19,** 3277 (1975).
7. C. D. Han and J. Y. Park, *J. Appl. Polym. Sci.,* **19,** 3291 (1975).
8. K. J. Choi, J. L. White, and J. E. Spruiell, *J. Appl. Polym. Sci.,* **25,** 2777 (1980).
9. T. Kanai and J. L. White, *Polym. Eng. Sci.,* **24,** 1185 (1984).
10. D. R. Holmes and R. P. Palmer, *J. Polym. Sci.,* **31,** 345 (1958).
11. P. H. Lindenmeyer and S. Lustig, *J. Appl. Polym. Sci.,* **9,** 227 (1965).
12. C. R. Desper, *J. Appl. Polym. Sci.,* **13,** 169 (1969).
13. E. Paschke, H. Ploenes, and H. Danz, *Kunstoffe,* **67,** 377 (1977).
14. W. F. Maddams and J. E. Preedy, *J. Appl. Polym. Sci.,* **22,** 2721 (1978).
15. W. F. Maddams and J. E. Preedy, *J. Appl. Polym. Sci.,* **22,** 2739 (1978).
16. W. F. Maddams and J. E. Preedy, *J. Appl. Polym. Sci.,* **22,** 2751 (1978).
17. W. F. Maddams and J. E. Preedy, *J. Appl. Polym. Sci.,* **22,** 3027 (1978).
18. M. A. Macrae and W. F. Maddams, *J. Appl. Polym. Sci.,* **22,** 2761 (1978).
19. T. Tagawa and K. Ogura, *J. Polym. Sci. Polym. Phys. Ed.,* **18,** 971 (1980).
20. K. J. Choi, J. E. Spruiell, and J. L. White, *J. Polym. Sci. Polym. Phys. Ed.,* **20,** 27 (1982).
21. E. S. Sherman, *Polym. Eng. Sci.,* **24,** 895 (1984).
22. A. Haber and M. R. Kamal, *ANTEC '87,* 446 (1987).
23. D. Parikh and G. Knight, *SPI/SPE Plast. West,* 87 (1987).
24. E. J. Dormier, J. M. Brady, W. H. Chang, S. D. Schregenberger, and J. D. Barnes. *ANTEC '89,* 696 (1989).
25. D. Hofmann, D. Geiss, A. Janke, G. H. Michler, and P. Fiedler, *J. Appl. Polym. Sci.,* **39,** 1595 (1990).
26. D. M. Simpson and I. R. Harrison, *ANTEC '93,* 1206 (1993).
27. K. C. H. Yi and N. J. Maraschin, *SP'90,* 89 (1990).

28. J. A. Ewen and H. C. Welborn, Jr., U.S. Pat. 4,530,914 (1985).
29. S.-B. Samuels and F. J. Karol, U.S. Pat. 4,918,038 (1990).
30. P. M. Stricklen, U.S. Pat. 4,939,217 (1990).
31. P. J. Flory and A. Vrij, *J. Am. Chem. Soc.*, **85,** 3548 (1963).
32. L. E. Alexander, *X-ray Diffraction Methods in Polymer Science,* Wiley, New York, 1969.
33. R. J. Pazur and R. E. Prud'homme, *J. Polym. Sci. Polym. Phys. Ed.*, **32,** 1475 (1994).
34. N. Brown and I. M. Ward, *J. Mater. Sci.*, **18,** 1405 (1983).
35. Z. W. Wilchinsky, *J. Appl. Phys.*, **31,** 1969 (1960).
36. D. I. Bower and W. F. Maddams, *The Vibrational Spectroscopy of Polymers,* Cambridge University Press, Cambridge, 1989.
37. G. Zerbi, G. Gallino, N. Del Fanti, and L. Baini, *Polymer,* **30,** 2324 (1989).
38. Y. V. Kissin, *J. Polym. Sci. Polym. Phys. Ed.*, **30,** 1165 (1992).
39. Z. Bashir, J. A. Odell, and A. Keller, *J. Mater. Sci.*, **19,** 3713 (1984).
40. Z. Bashir, J. A. Odell, and A. Keller, *J. Mater. Sci.*, **21,** 3993 (1986).

Received June 15, 1995
Accepted March 30, 1996